ELSEVIER

Nuclear Instruments and Methods in Physics Research B 186 (2002) 281–286

NIM B
Beam Interactions with Materials & Atoms

www.elsevier.com/locate/nimb

Modeling of the Ostwald ripening of extrinsic defects and transient enhanced diffusion in silicon

A. Claverie [a,*], B. Colombeau [a], F. Cristiano [b], A. Altibelli [a], C. Bonafos [a]

[a] *Ion Implantation Group, CEMES/CNRS, BP 4347, F-31055 Toulouse Cedex 4, France*
[b] *LAAS/CNRS, 7 Avenue du Colonel Roche, F-31077 Toulouse Cedex, France*

Abstract

We present an atomistic simulation of the Ostwald ripening of extrinsic defects (clusters, {1 1 3}s and dislocation loops) which occurs during annealing of ion implanted silicon. The model describes the capture and emission of Si interstitial atoms to and from extrinsic defects of sizes up to thousands of atoms and includes a loss term due to the flux of interstitials to the recombining surface. Key input parameters of the simulation are the variations of the formation energy and of the capture efficiency with the size of the different defects. This model shows that the kinetics of the well-known dissolution of {1 1 3} defects is only driven by the recombination efficiency at the surface and the distance from the defects to the sample surface. We have subsequently used this model to study defect evolution in low and ultra low energy (ULE) B implanted Si during annealing. Defect dissolution occurs earlier and at smaller sizes in the ULE regime. Consequently, TED is mostly characterized by its ''pulse'' component which occurs at the very beginning of the anneal.

Keywords: Semiconductors; Nanoparticles; Extended defects; Ostwald ripening; Atomistic simulations

1. Introduction

The predictive simulation of dopant diffusion in Si is essential for the controlled reduction of the dimensions of future ICs. Among other dopants, boron is of special importance since the diffusion anomalies it experiences during annealing ultimately determines the electrical characteristics of the junctions. There are two distinct components in the anomalous diffusion of boron in Si. On the one hand, for both high concentrations of B and Si interstitial atoms, boron–Si interstitial clusters (BICs) are formed and tend to immobilise a fraction of B. On the other hand, the coupling of free-interstitial Si atoms with (probably) substitutional boron atoms enhances the B diffusivity by a factor which is proportional to the supersaturation of Si interstitials in the region. Thus, describing and modelling boron diffusion requires the knowledge of the time and space evolution of the Si(int)s supersaturation in the region where B remains during annealing. Ion implantation and/or dopant activation itself results in the generation or large quantities of point defects, namely vacancies and interstitials, the latter species always being in excess to the former. At room temperature, these

* Corresponding author. Tel.: +33-5-62-25-79-00; fax: +33-5-62-25-79-99.
E-mail address: claverie@cemes.fr (A. Claverie).

0168-583X/02/$ - see front matter
PII: S0168-583X(01)00914-4

defects are not stable and migrate until they recombine and form more stable species involving two or more Si atoms or vacancies [1]. During annealing, these defects totally recombine until only small Si aggregates are left which grow in size. Earlier works have ascribed the diffusivity enhancement of boron to the release of Si atoms by one type of such extended defect, namely the {1 1 3}s [2,3]. However, it has since been shown that the formation and dissolution of these defects is not a pre-requisited condition for the occurrence of TED since TED is also observed when {1 1 3}s transform into dislocation loops [4] or are not formed at all [5]. Recently a much better understanding of the thermal behavior of all these extended defects has been gained and the driving force for their evolution has been clearly identified [6,7]. The goal of this paper is to show how the modelling of the defect evolution in Si based on such new concepts allows one to describe well-known experimental results concerning the kinetics of extended defects during annealing. Moreover, this model describes the concomitant behavior of the Si interstitial atoms in the region, i.e. calculates the source term for TED. In particular, we will use our simulations to explain the specifics of TED observed after ultra low energy (ULE) implants.

2. Material science background

Depending on experimental conditions, up to 4 types of extrinsic, i.e. interstitial-type extended defects can be detected by TEM [6]. They range, depending on the number of Si atoms they contain, from clusters of about 2 nm in size, to {1 1 3} defects and to dislocation loops of two types. All these defects are "precipitates" of Si atoms which evolve in size but also in shape and crystallographical characteristics during annealing. The basic mechanism at the origin of their evolution is a competitive growth in which the defects interchange Si atoms through matrix diffusion with rates that depend on the defect stability i.e. their formation energy and their ability to capture Si atoms. Because of this interchange, the region where the defects evolve is oversaturated with free Si interstitial atoms. A dynamical equilibrium exists between this supersaturation "mean field" and the population of defects. The phenomenon can be conservative or not depending upon the eventual presence of a strong sink for Si interstitial in the vicinity of this mean-field. In such cases, for example when the initial excess of Si atoms is close enough to the surface of the wafer and/or when the annealing ambient promotes fast recombination of Si(int)s at the surface, the loss of interstitials, i.e. the dissolution of the defects before their transformation into more stable forms, can occur. Such a competitive growth is named Ostwald ripening and has been initially developed to describe the growth of liquid droplets in equilibrium with their vapor. The Gibbs–Thomson equation expresses the key concept needed to model this phenomenon and is currently used to describe the nucleation and growth of various particles in solid matrices [8].

3. Atomistic simulation of defect growth

The atomistic approach describes the growth of precipitates in a matrix by calculating the difference between the capture (F_n) and emission (R_n) rates of every cluster of size n. The growth rate is classically written as the product of the capture area of the particle by the net flux of atoms towards it. In the case of a diffusion-limited growth, this growth rate can be written [8] as

$$\frac{\mathrm{d}n}{\mathrm{d}t} = |F_n - R_n| D_\mathrm{i} C_\mathrm{i}^* A_n \left.\frac{\mathrm{d}S}{\mathrm{d}R}\right|_{R=r} = D_\mathrm{i} C_\mathrm{i}^* \frac{A_n}{R_\mathrm{eff}} (\overline{S} - S(n)), \quad (1)$$

where $D_\mathrm{i} C_\mathrm{i}^*$ is the self-diffusivity of the impurity atoms within the host matrix. A_n is the capture area of the precipitate. Because R_eff represents the radial extension of the diffusion field, A_n/R_eff characterises the capture efficiency of the defect. $\overline{S}$ is the mean supersaturation of these Si interstitials within the matrix and $S(n)$ is the supersaturation of interstitials in equilibrium with a precipitate containing n atoms. $S(n)$ is given by the Gibbs–Thomson equation and can be written as

$$S(n) = \exp\left[\frac{E_\mathrm{f}(n)}{kT}\right], \quad (2)$$

where $E_f(n)$ being the formation energy (the derivative of the total energy) of a precipitate containing n atoms. The emission rate (R_n) is thus proportional to the formation energy of the particle and is given by

$$R_n = D_i C_i^* \frac{A_n}{R_{eff}} \exp\left(\frac{E_f(n)}{kT}\right). \quad (3)$$

The capture rate (F_n) is a function of the environment of the precipitate and is proportional to $\overline{S}$, the mean supersaturation of Si interstitials between the precipitates,

$$F_n = D_i C_i^* \frac{A_n}{R_{eff}} \overline{S}. \quad (4)$$

Both the capture efficiency (A_n/R_{eff}) and the formation energy (E_f) depend on the geometry of the defect.

The atomistic model is based on a set of $(n+1)$ coupled differential equations. The first n equations describe the flux of atoms from particles of size (n) to particles of size $(n+1)$ and $(n-1)$,

$$\frac{dN_n}{dt} = F_{n-1}N_{n-1} - F_nN_n + R_{n+1}N_{n+1} - R_nN_n. \quad (5)$$

This equation drives the growth of the defects both in terms of sizes and densities. (Eq. 6) describes the "free component" of the Si atoms i.e. the concomitant evolution of the free Si interstitials supersaturation in dynamical equilibrium with the extended defects,

$$\overline{S} = \frac{\sum_{n=2}^{\infty} \beta_n R_n N_n}{D_i C_i^* \left(\left(\sum_{n=2}^{\infty} \frac{A_n}{R_{eff}} N_n\right) + \frac{1}{L_{surf} + r_p}\right)}, \quad (6)$$

where N_n is the number of precipitates of size n. L_{surf} is the recombination length at the surface and r_p the depth position of the defects. The quantity β is the number of Si atoms released by the break-up of a cluster ($\beta = 2$ for $n = 2$, $\beta = 1$ otherwise). Eq. (6) describes the time evolution of the supersaturation mean-field centered on the defects and at the origin of TED.

The difficulty when trying to simulate the nucleation and growth of interstitial type defects in silicon lies in the various different geometries these defects can adopt. Indeed, from clusters to {1 1 3}s and then to dislocations loops (of two types), four main different types of precipitate may coexist with their own capture efficiencies and size-dependent formation energies. However, for the results presented in this paper, we restrict ourselves to the situation where "only" defects up to large {1 1 3}s can be formed i.e. for the case of non-amorphising implants.

For cluster sizes of up to 10 atoms, we take the experimentally deduced oscillating formation energies from Cowern [9] with stable configurations for 4 and 8 atoms. For larger sizes, we tend towards the values expected for small {1 1 3} defects. In order to access to the formation energies of the {1 1 3}s, we have calculated the total energy of these defects based on their crystallographical characteristics i.e. taking into account the two edge dislocations plus the two mixed dislocations plus the stacking fault energy which together define this defect [10]. They have been assumed to be planar, rectangular and of constant width (4 nm). They contain 20 atoms per nm. Fig. 1 shows the variation of the formation energy of these defects as a function of their size. This energy curve gently tends towards its asymptotical limit at 0.65 eV [10].

Since little is known of the structure of the clusters, we have reasonably assumed that they are spherical and that their capture area is $An = 4\pi r^2$, where r is the geometrical radius of the cluster. Approaching the capture area of a {1 1 3} defect is far more difficult. Gencer and Dunham [11] have proposed that capture occurs only through the edges of these elongated defects. We prefer to

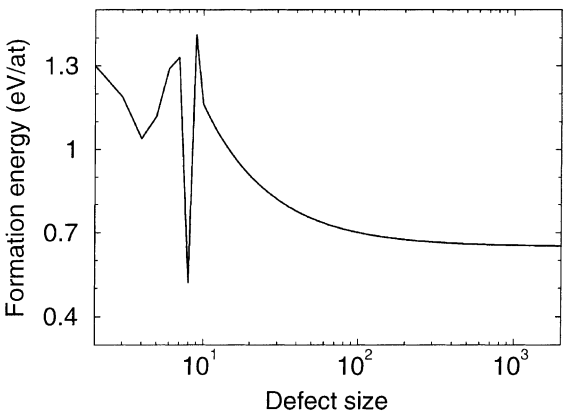

Fig. 1. Variation of the formation energies of clusters and {1 1 3}s as a function of the number of Si atoms they contain.

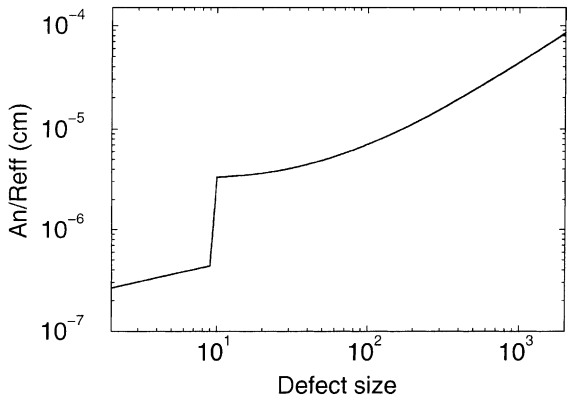

Fig. 2. Variation of the capture efficiency of clusters and {1 1 3}s as a function of the number of Si atoms they contain.

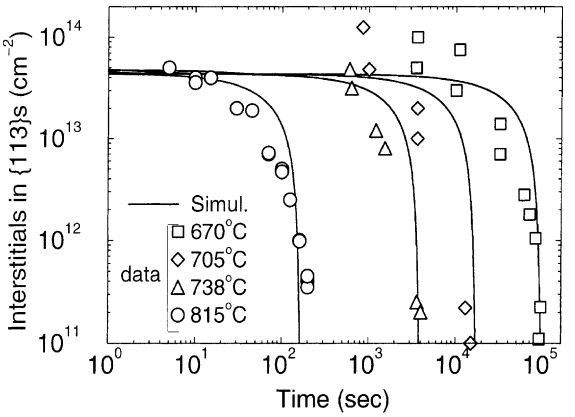

Fig. 3. Dissolution kinetics of {1 1 3}s: comparison between TEM results and simulations.

assume that the capture area offered by this type of elongated defects. still increases as they become longer. Thus, our capture area is the sum of three terms (i) the two cylinders at the width sides, (ii) the two cylinders along the length sides and (iii) the four hemispheres at the corners. The overall variation of the capture efficiency A_n/R_{eff} is shown in Fig. 2. The exact amplitude and position of the abrupt jump corresponding to the transition from spherical to elongated precipitates have little impact on the results shown in the next section. All simulations were run with the $D_{\text{i}}C_{\text{i}}^{*} = 2 \times 10^{24}$ $\exp(-4.52/kT)$ cm^{-1}/s as deduced from Cowern's experiments [9].

4. Results

We have tested the model using two notorious experimental studies of defect evolution. The first set concerns the dissolution of the {1 1 3}s initially observed by Eaglesham et al. [2]. Fig. 3 shows the comparison between our simulation and a compilation of their experimental results [2,3]. An excellent fit is obtained by adjusting only $(L_{\text{surf}} + r_{\text{p}})$ at 80 nm in Eq. (6). Clearly, these simulations show that the occurrence of defect dissolution depends only on the distance and sink efficiency of the surface. The growth of the defects, i.e., the size increase and density decrease they experience during this non-conservative Ostwald ripening, perfectly matches the experimental observations (not shown) and this evolution strongly depends on the size dependence of the formation energy of the defects. While the model is able to describe the "frozen" component of the Si interstitials i.e. the growth of defects, its ability to describe the diffusive behavior of boron has to be tested. For this purpose, we recall a recent experiment by Cowern et al. [9] in which the diffusivity of CVD grown boron delta layers after low dose Si implantation was studied during low temperature annealing. The time variation of the boron diffusivity enhancement i.e. of the Si supersaturation, was extracted from these experiments and are plotted in Fig. 4 along with the results of our simulations. At

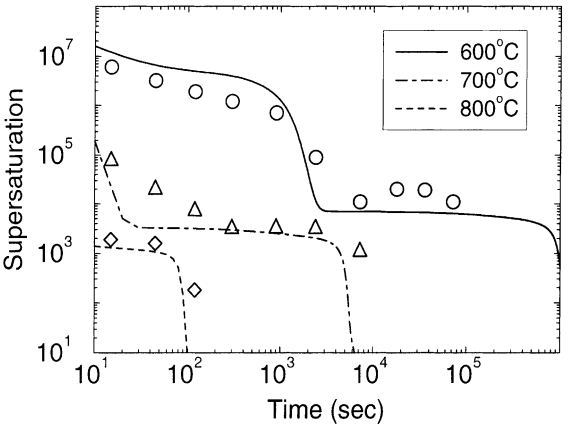

Fig. 4. Time variation of the supersaturation of Si(int)s during annealing: comparison between "marker" experiments and simulations.

low temperature, our simulations reproduce well the two observed plateaus involving firstly the stable clusters with 4 and 8 atoms and then the {1 1 3} defects. At higher temperature, the evolution is faster and only the {1 1 3}s survive long enough to be detected at this time scale. Such fits between experiments and simulations cannot be obtained without assuming the presence of at least two efficient traps in the 2–10 atoms range.

Having gained some confidence on the ability of our model to describe *both* defect growth and Si supersaturation evolution, we now study through computer simulation the effect of reducing the energy of a boron implant in Si from 25 to 1 keV, at a constant dose of 10^{14} ions/cm^2. For this, we assume that the "+1" model holds and we "anneal" these implants at 950 °C. Fig. 5(a) and (b) show the time evolution of the mean size and of the density, respectively, of the defects for the four different implants. Up to 35 nm-long {1 1 3}s are produced after 2 s annealing of the 25 keV implant, which quickly reduce in size and density for longer annealing times. This agrees well with TEM observations. Moreover, as the implant energy decreases, the maximum size that the defects can reach before dissolution decreases. While defects large enough to be detected by TEM can still be formed after lower energy implants, they typically dissolve after 0.1–1 s, i.e. probably during the ramping up of the anneal. Fig. 5(c) shows the time evolution of the number of interstitials stored in the defects. Reducing the implant energy from 25 to 5 KeV affects the time after which dissolution starts. The overall number of atoms initially stored in the defects is almost independent of the energy in this energy range and is close to the implanted dose.

In contrast, after 1 keV implantation, the surface pumps the free interstitial supersaturation at the very beginning of the cluster growth and thus

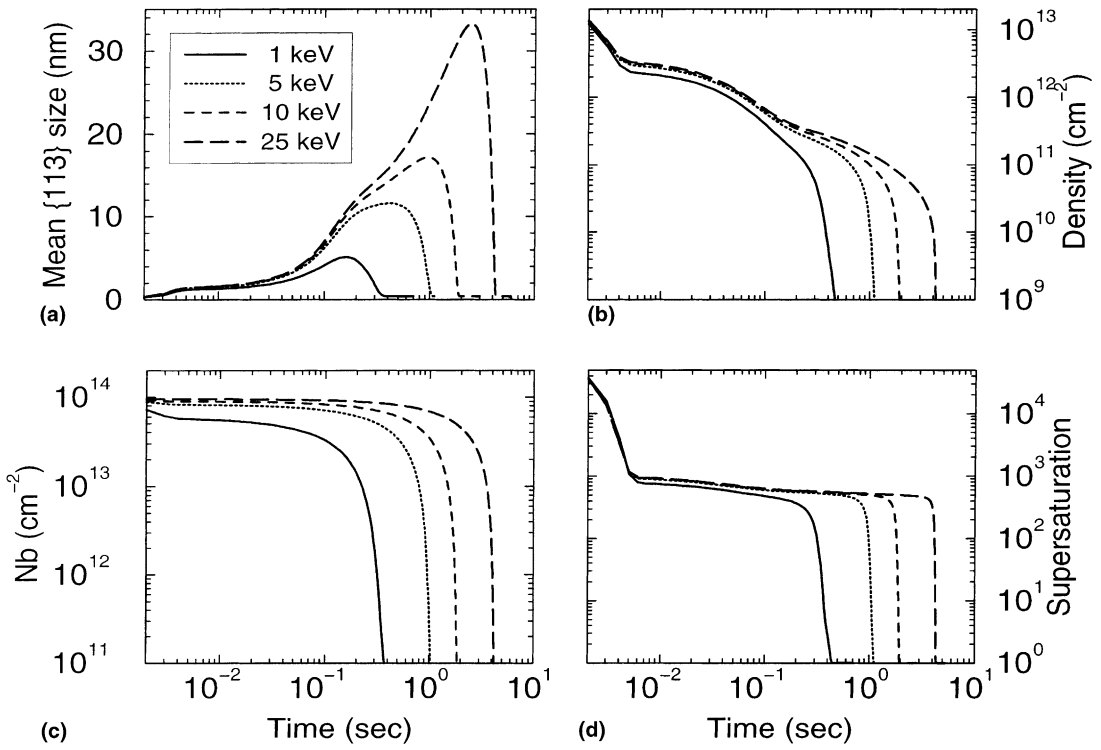

Fig. 5. Simulation of the annealing at 950 °C of 1×10^{14} ions/cm^2 boron implants in the 25–1 keV range. Time evolutions of (a) mean size of the defects; (b) defect density; (c) total number of Si atoms stored in the defects (Nb); (d) Si(int)s supersaturation in the defect region.

the total number of Si(int)s stored in the defects is significantly smaller than observed after higher energy implants. Finally, Fig. 5(d) shows the evolution of the Si(int)s supersaturation in the defect region following implantation in this energy range. At very short times (<0.01 s), the supersaturation shows a "pulse" when only clusters of small sizes exist and rapidly evolve towards {1 1 3}s or dissolve. For longer times, a large plateau is observed and corresponds to the dynamical equilibrium between the supersaturation mean field and the {1 1 3} defects. It is important to note that for the 1 keV implant, the pulse component represents near about 40% of the overall diffusivity enhancement boron will experience during a classical annealing. Since this pulse is driven by small clusters of high formation energies, this explains why the measured activation energy for TED is much smaller after ULE implants (ultrafast TED) than after higher energy implants.

5. Conclusions

A physical based modeling of the growth of extended defects resulting from the precipitation of excess Si interstitial atoms has been presented. This model describes the non-conservative Ostwald ripening of precipitates in a matrix in the presence of a strong sink. It allows the dissolution of {1 1 3}s to be simulated and moreover gives access to the concomitant evolution of the supersaturation of Si(int)s in the defect region. This supersaturation is the "source term" which is needed in process simulators to account for the diffusivity enhancements observed during annealing of ion implanted silicon.

References

[1] K.L. Brower, Phys. Rev. B 14 (1976) 872.
[2] D.J. Eaglesham, P.A. Stolk, H.J. Gossmann, J.M. Poate, Appl. Phys. Lett. 65 (1994) 2305.
[3] P.A. Stolk, H.J. Gossmann, D.J. Eaglesham, D.C. Jacobson, C.S. Rafferty, G.H. Gilmer, M. Jaraiz, J.M. Poate, H.S. Luftman, T.E. Haynes, J. Appl. Phys. 81 (1997) 6031.
[4] J. Li, K.S. Jones, Appl. Phys. Lett. 73 (1998) 3748.
[5] L.H. Zhang, K.S. Jones, P.H. Chi, D.S. Simons, Appl. Phys. Lett. 67 (1995) 2025.
[6] A. Claverie, B. Colombeau, G. Ben Assayag, C. Bonafos, F. Cristiano, M. Omri, B. de Mauduit, Mater. Sci. Semicond. Proc. 3 (2000) 269.
[7] A. Claverie, F. Cristiano, B. Colombeau, N.E.B. Cowern, Mater. Res. Soc. Proc., in print.
[8] C. Bonafos, B. Colombeau, A. Altibelli, M. Carrada, G. Ben Assayag, B. Garrido, M. López, A. Pérez-Rodríguez, J.R. Morante, A. Claverie, Nucl. Instr. and Meth. B 178 (2001) 17.
[9] N.E.B. Cowern, G. Mannino, P.A. Stolk, F. Roozeboom, H.G.A. Huizing, J.G.M. van Berkum, F. Cristiano, A. Claverie, M. Jaraiz, Phys. Rev. Lett. 82 (1999) 4460.
[10] B. Colombeau, F. Cristiano, C. Bonafos, A. Claverie, to be published.
[11] A.H. Gencer, S.T. Dunham, J. Appl. Phys. 81 (1997) 631.